行政院國家科學委員會專題研究計畫 成果報告

超導體的二個問題與光子晶體性質的研究
研究成果報告(精簡版)

計 畫 類 別 ：個別型
計 畫 編 號 ：NSC 96-2112-M-216-001-
執 行 期 間 ：96 年 08 月 01 日至 97 年 08 月 31 日
執 行 單 位 ：中華大學電機工程學系

計 畫 主 持 人 ：楊宗哲

報 告 附 件 ：國外研究心得報告
出席國際會議研究心得報告及發表論文

處 理 方 式 ：本計畫可公開查詢

中 華 民 國 97 年 10 月 22 日

Effect of atomic position on the spontaneous emission of a three-level atom in a coherent photonic-band-gap reservoir

Szu-Cheng Cheng,[1,*] Jing-Nuo Wu,[2,†] Tzong-Jer Yang,[3] and Wen-Feng Hsieh[2]
[1]*Department of Physics, Chinese Culture University, Taipei, Taiwan, Republic of China*
[2]*Department of Photonics, National Chiao Tung University, Hsinchu, Taiwan, Republic of China*
[3]*Department of Electrical Engineering, Chung Hua University, Hsinchu, Taiwan, Republic of China*
(Received 10 May 2008; revised manuscript received 6 September 2008; published 5 January 2009)

The effect of atomic position on the spontaneous emission and optical spectra of a three-level atom embedded in a photonic crystal was studied by considering the coherent two-band photonic-band-gap (PBG) reservoir. With the definite phase difference between the fields of the air band and dielectric band in this coherent PBG reservoir, we found that this coherent property grows stronger and results in the spectrum shift and the appearance of dark lines and kinks as the width of band gap gets smaller; and the variation of the atomic position leads to large shift of spectral peak. The averaged spectra of the system with an ensemble of atoms embedded in the dielectric region are blueshifted while those of atoms in the air region are redshifted. The spectra peaks can even shift more than 75% of the half width at half maximum. The feasible experimental systems composed of an ensemble of molecules (quantum dots or fluorescence dye) in photonic crystals are discussed.

DOI: 10.1103/PhysRevA.79.013801 PACS number(s): 42.50.Gy, 42.70.Qs

I. INTRODUCTION

It is well known that spontaneous emission (SE) rate and optical properties of atoms can be modified effectively by placing the atoms in photonic band gap (PBG) materials [1–10], where the density of modes of the reservoirs has significant deviation from that of free space vacuum. This modification changes the atomic coherence and quantum interference effects and provides potential application to quantum optical communication. The related atomic coherence effects include the electromagnetically induced transparency (EIT) [11], lasing without inversion [12,13], slow propagation of light [14], and nonlinear effects at low light level [15].

Here we propose a different point of view on varying the SE and optical resonant spectra through changing the relative position of the embedded atom in photonic crystals (PCs). It originates from the fact that the strength of photon-atom interaction depends on the atomic position [16] and the two-band reservoir becomes coherent and can interfere with each other, which results from the definite phase difference between the air-band and dielectric-band fields of PBG [17]. One band approximation is valid when the PBG is relatively wide and the transition frequencies of the atoms is near the air or dielectric band edge. For the photonic crystals with narrow band gap, the photon-atom coupling between the embedded atom and the system has to consider the contribution of both electric fields from the air-band and dielectric-band reservoirs. Existence of both reservoirs leads to a stronger photon-atom coupling [16], and the time evolution decay of the excited population of a two-level atom has been shown faster than that in the one-band approximation. Although atomic coherence in a Λ-type three-level atom embedded in a PBG structure has been studied using the two-band model [18–20], it was assumed that the atom inside PCs interacted with two incoherent PBG reservoirs. The results of Ref. [18] revealed that the photon-atom coupling strengths of both reservoirs were the same and independent of the position of the embedded atom. In this paper, a Λ-type three-level atom embedded in a PBG structure is studied (Fig. 1). One transition level of the atom ($|2\rangle \leftrightarrow \langle 1|$) lies near the PBG edge; the other transition ($|2\rangle \leftrightarrow \langle 0|$) is far from the PBG edge and couples with the Markovian reservoir. We investigate the spontaneous emission spectrum of atoms in the PBG reservoir with a coherent property, which depends on the embedded position of the atom and the width of the band gap. The variation of the atomic position and band-gap width would lead to the change of the SE rate and the spectra of absorption and dispersion. These results provide a new degree of freedom to vary the SE and optical properties in PCs, especially for nonlinear optical phenomena.

This paper is organized as follows. In Sec. II, we derive the atom-field coupling Hamiltonian, where the position dependence of the atom-field coupling constants is considered, and show that this position dependence of the atom-field couplings is induced by the phase difference of the air-band and dielectric-band fields at different locations of the embedded atom. In Sec. III, we apply the Schrödinger picture to describe the interaction of the embedded atom with the PBG reservoir. We then calculate the SE spectrum in the free space vacuum and discuss it under the different band-gap widths and relative positions of the atom. In Sec. IV, we discuss the optical properties of the system by adding a weak probe laser to the system. Absorption and dispersion spectra of the system are studied. Finally, we summarize our results in Sec. V.

II. ATOM-FIELD COUPLING HAMILTONIAN

Considering the system of an excited atom embedded in a photonic crystal under the Coulomb gauge $\nabla \cdot \vec{A} = 0$, one can

*FAX: +886-2-28610577. sccheng@faculty.pccu.edu.tw
†FAX: +886-3-5716631. jingnuowu@so-net.net.tw

write the interaction Hamiltonian of the atom with a radiation field as

$$H = -\frac{e}{m}\vec{P}\cdot\vec{A}_{PC}, \tag{1}$$

where e and m are the charge and mass of single electron in the atom, $\vec{P}$ is the momentum of the electron without spin, and the radiation field for the reservoir of a photonic crystal is described by the quantized vector potential $\vec{A}_{PC}$. This vector potential can be expressed as [16]

$$\vec{A}_{PC}(\vec{r}_0,t) = \sum_n \int_{BZ} \frac{d\vec{k}}{(2\pi)^3}\sqrt{\frac{\hbar}{2\epsilon_0\omega_{n,\vec{k}}V}} \times[\vec{A}_{n,\vec{k}}(\vec{r}_0)\hat{a}_{n,\vec{k}}e^{-i\omega_{\vec{k}}t} + \vec{A}^*_{n,\vec{k}}(\vec{r}_0)\hat{a}^+_{n,\vec{k}}e^{i\omega_{\vec{k}}t}], \tag{2}$$

where V is the volume of a unit cell of the lattice, ϵ_0 is the Coulomb constant, n is the energy band index in the first Brillouin zone representing the air band by a and the dielectric band by d, and the integral is over each band in this region of $\vec{k}$ space. In addition, $\hat{a}^+_{n,\vec{k}}$ and $\hat{a}_{n,\vec{k}}$ are the creation and annihilation operators for a field mode with energy band index n, wave vector $\vec{k}$, and frequency $\omega_{\vec{k}}$. Here the Bloch modes $\vec{A}_{n,\vec{k}}$ satisfy the Bloch-Floquet theorem $\vec{A}_{n,\vec{k}}(\vec{r}_0+\vec{R}) = e^{i\vec{k}\cdot\vec{R}}\vec{A}_{n,\vec{k}}(\vec{r}_0)$ and a reduced zone scheme for $\vec{k}$ is adopted. If only dipole contribution of the electronic charge distribution is considered, the interaction Hamiltonian for the field modes in PCs could be expressed as [2]

$$H_{PC} \approx -\frac{e}{m}\vec{P}\cdot\vec{A}_{PC}(\vec{r}_0,t) = -i\hbar\sum_{n,\vec{k}} g_{n,\vec{k}}(|j\rangle\langle i|\hat{a}_{n,\vec{k}}e^{-i\omega_{\vec{k}}t} - \hat{a}^+_{n,\vec{k}}e^{i\omega_{\vec{k}}t}|i\rangle\langle j|), \tag{3}$$

where $g_{n,\vec{k}} = \frac{\omega_{ij}}{\hbar}\left(\frac{\hbar}{2\epsilon_0\omega_{\vec{k}}V}\right)^{1/2}\vec{d}_{ij}\cdot\vec{E}^*_{n,\vec{k}}(\vec{r}_0)$ is the position-dependent coupling strength of the atom with the photonic crystal field modes (n), $\vec{d}_{ij}$ is the atomic dipole moment for the transition $|i\rangle\rightarrow|j\rangle$ with basis vectors $\{|i\rangle\}$ forming a complete orthogonal set of the atomic system, and $\omega_{ij}=\omega_i-\omega_j$ is the atomic transition frequency between levels $|i\rangle$ and $|j\rangle$. Note that $\vec{r}_0$ is designated to be the position of the atomic nucleus. We shall assign $\vec{E}^*_{a,\vec{k}}(\vec{r}_0)$ and $\vec{E}^*_{d,\vec{k}}(\vec{r}_0)$ as the atom-coupling fields from the air band and dielectric band, respectively.

In discussing the physical origin of the PBG, Joannopoulos *et al.* [17] applied the electromagnetic variational theorem and found that the low-frequency modes concentrate their energy in the high dielectric constant regions and the high-frequency modes in the low dielectric regions. Since the low dielectric regions are often air regions, they therefore refer to the high-frequency modes as the "air band" and the low-frequency modes as the "dielectric band." The PBG (frequency difference) arises due to this difference in field energy location. The corresponding distributions of electric fields of one-dimensional photonic crystals are plotted in Figs. 2(a) and 2(b). These distributions of electric fields from the two-band reservoir are two coherent waves with $\pi/2$ phase difference and can thus be given by

$$\vec{E}^*_{a,\vec{k}}(\vec{r}_0) = E_{\vec{k}}\cos\theta(\vec{r}_0)\hat{\epsilon}, \quad \vec{E}^*_{d,\vec{k}}(\vec{r}_0) = E_{\vec{k}}\sin\theta(\vec{r}_0)\hat{\epsilon}, \tag{4}$$

where $\hat{\epsilon}$ is a unit vector of the electric field, the angle parameter $\theta(\vec{r}_0)$ "sees" by the active atom located at $\vec{r}_0$ within a unit cell [21], and a single amplitude $E_{\vec{k}}$ is contained in these two coherent eigenmode fields. The position-dependent effect on the atom-field coupling is thus constructed to illustrate the connection of the atomic actual position with angle parameter $\theta(\vec{r}_0)$ [22]. This effect is absent in the previous two-band model [23], in which two independent eigenmode fields were used for the two-band reservoir. Notice that our two-band model reduces to the single-band model as $\theta(\vec{r}_0)=0$ (or $\frac{\pi}{2}$).

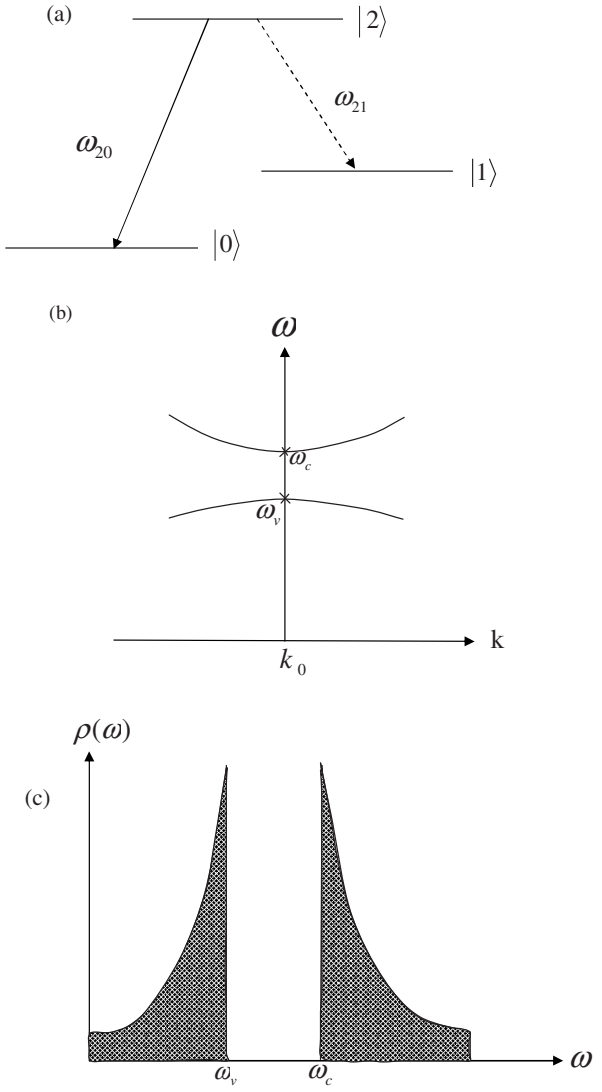

FIG. 1. (a) A Λ-type three-level atom with excited state $|2\rangle$, intermediate state $|1\rangle$, and ground state $|0\rangle$. The transition frequency ω_{21} lies near the PBG edges and ω_{20} far from the PBG edges. (b) Dispersion relation near the PBG edge with ω_c and ω_v being the air-band and dielectric-band edge frequencies. (c) Density of states (DOS) of the two-band isotropic effective mass model.

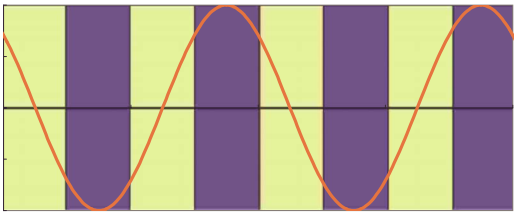
(a)

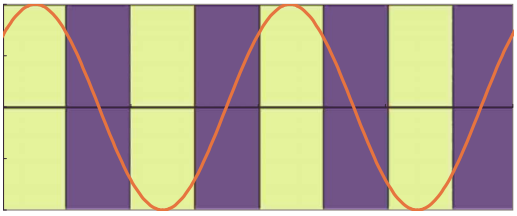
(b)

FIG. 2. (Color online) (a) The electric field profile of dielectric-band modes and (b) air-band modes from the two-band reservoir of one-dimentional photonic crystals. The high-dielectric region is in blue (darker) color and low-dielectric region in yellow (faint) color.

III. SPONTANEOUS EMISSION IN THE FREE-SPACE RESERVOIR

Consider a Λ-type three-level atom, whose energy diagram is shown in Fig. 1, being embedded inside a PBG structure. The atom is assumed to be initially excited in state $|2\rangle$. The transition between $|2\rangle \leftrightarrow \langle 1|$ is considered to be near resonant with the band edge of the PBG reservoir, while the transition between $|2\rangle \leftrightarrow \langle 0|$ is assumed to be far away from the PBG edge, and is coupling with the free-space reservoir.

In a rotating-wave approximation, the interaction Hamiltonian for a three-level atom and the electromagnetic field in a photonic crystal can be written as

$$H = \hbar \sum_{\lambda} g_{\lambda} e^{-i(\omega_{\lambda}-\omega_{20})t} |2\rangle\langle 0|\hat{a}_{\lambda} + \hbar \sum_{a} g_a(\vec{r}_0) e^{-i(\omega_a-\omega_{21})t} |2\rangle\langle 1|\hat{a}_a + \hbar \sum_{d} g_d(\vec{r}_0) e^{-i(\omega_d-\omega_{21})t} |2\rangle\langle 1|\hat{a}_d + \text{H.c.} \quad (5)$$

Here g_{λ} characterizes the coupling constant of the atom with the free-space vacuum modes λ while the position-dependent coupling strength of the atom with the air (dielectric) -band-reservoir modes a (d) has the form of

$$g_{a(d)}(\vec{r}_0) = \frac{\omega_{21}}{\hbar}\left[\frac{\hbar}{2\epsilon_0 \omega_{a(d)} V}\right]^{1/2} \vec{d}_{21} \cdot \vec{E}^{*}_{a(d)}(\vec{r}_0). \quad (6)$$

We denoted the atomic transition frequency as ω_{ij} photonic eigenmode frequency as $\omega_{a(d)}$, and fixed polarization orientation of atomic dipole moment $\vec{d}_{21}$ [24].

In the single photon sector, the wave function of the system could be described as

$$|\Psi(t)\rangle = \alpha_2(t)|2,\{0_{\lambda},0_a,0_d\}\rangle + \sum_{\lambda} \alpha_{0\lambda}(t)|0,\{1_{\lambda},0_a,0_d\}\rangle + \sum_{a} \alpha_{1a}(\vec{r}_0,t)|1,\{0_{\lambda},1_a,0_d\}\rangle + \sum_{d} \alpha_{1d}(\vec{r}_0,t)|1,\{0_{\lambda},0_a,1_d\}\rangle. \quad (7)$$

Here $\alpha_2(t)$ and $\alpha_{0\lambda}(t)$ are the probability amplitudes of the system in the states $|2,\{0_{\lambda},0_a,0_d\}\rangle$ and $|0,\{1_{\lambda},0_a,0_d\}\rangle$, which describe the atom in the state $|2\rangle$ with no photon and in the state $|0\rangle$ with a single photon in the mode λ, respectively. The probability amplitudes of the system in the states $|1,\{0_{\lambda},1_a,0_d\}\rangle$ and $|1,\{0_{\lambda},0_a,1_d\}\rangle$ (the atom in the state $|1\rangle$ and a photon in either the air or dielectric band) are considered to be functions of atomic position and assumed to be

$$\alpha_{1a}(\vec{r}_0,t) = \alpha_{1\vec{k}}(t)\cos\theta(\vec{r}_0), \quad \alpha_{1d}(\vec{r}_0,t) = \alpha_{1\vec{k}}(t)\sin\theta(\vec{r}_0). \quad (8)$$

This assumption comes from the position-dependent electric fields of the two-band reservoir and makes the probability of the system in atomic level $|1\rangle$ to be $|\alpha_{1\vec{k}}(t)|^2$.

As the SE rate is studied, we assume the atom is initially excited in state $|2\rangle$. By substituting the interaction Hamiltonian and single-photon wave function into the time-dependent Schrödinger equation, we have the time evolution of the probability amplitudes,

$$i\frac{d}{dt}\alpha_2(t) = \sum_{\lambda} g_{\lambda}\alpha_{0\lambda}(t)e^{-i(\omega_{\lambda}-\omega_{20})t} + \sum_{a} g_a(\vec{r}_0)\alpha_{1a}(\vec{r}_0,t)e^{-i(\omega_a-\omega_{21})t} + \sum_{d} g_d(\vec{r}_0)\alpha_{1d}(\vec{r}_0,t)e^{-i(\omega_d-\omega_{21})t}, \quad (9)$$

$$i\frac{d}{dt}\alpha_{0\lambda}(t) = g_{\lambda}\alpha_2(t)e^{i(\omega_{\lambda}-\omega_{20})t}, \quad (10)$$

$$i\frac{d}{dt}\alpha_{1a}(\vec{r}_0,t) = g_a(\vec{r}_0)\alpha_2(t)e^{i(\omega_a-\omega_{21})t}, \quad (11)$$

$$i\frac{d}{dt}\alpha_{1d}(\vec{r}_0,t) = g_d(\vec{r}_0)\alpha_2(t)e^{i(\omega_d-\omega_{21})t}. \quad (12)$$

Combining these equations with position-dependent coupling strength and probability amplitudes [Eqs. (6) and (8)], we obtained the integrodifferential equation

$$\frac{d}{dt}\alpha_2(t) = -\sum_{\vec{k}} g^2_{\vec{k}} \int_0^t d\tau \alpha_2(\tau) \times[\sin^2\theta e^{-i(\omega_d-\omega_{21})t} + \cos^2\theta e^{-i(\omega_a-\omega_{21})t}] \times [\sin^2\theta e^{i(\omega_d-\omega_{21})\tau} + \cos^2\theta e^{i(\omega_a-\omega_{21})\tau}] - \sum_{\lambda} g^2_{\lambda} \int_0^t d\tau \alpha_2(\tau) e^{-i(\omega_{\lambda}-\omega_{20})(t-\tau)}, \quad (13)$$

where we have approximated $g_a(\vec{r}_0) \cong g_{\vec{k}} \cos\theta(\vec{r}_0)$ and $g_d(\vec{r}_0) \cong g_{\vec{k}} \sin\theta(\vec{r}_0)$ with real constant $g_{\vec{k}} = \frac{\omega_{21}}{\hbar}(\frac{\hbar}{2\epsilon_0\omega_{\vec{k}}V})^{1/2} E_{\vec{k}}(\vec{d}_{21}\cdot\hat{\epsilon})$ which agrees with the case of single amplitude for electric fields. The first summation reveals the quantum interference of two atomic-emission channels along with the two-band PBG reservoir ($\omega_{21} \cong \omega_a$ and $\omega_{21} \cong \omega_d$). It could be further dealt with by defining the the memory functions (or kernels) from the PBG reservoir as

$$K_1(t) = \sum_{\vec{k}} g_{\vec{k}}^2 e^{-i(\omega_d-\omega_{21})t} = \beta^{3/2} \int d\omega \rho_d(\omega) e^{-i(\omega-\omega_{21})t},$$

$$K_2(t) = \sum_{\vec{k}} g_{\vec{k}}^2 e^{-i(\omega_a-\omega_{21})t} = \beta^{3/2} \int d\omega \rho_a(\omega) e^{-i(\omega-\omega_{21})t}, \tag{14}$$

where β is the coupling constant of the atom-reservoir system and $\rho(\omega)$ is the density of modes of the reservoir. When the two-band isotropic effective mass model of the PBG reservoir is considered, we have the density of modes [see Fig. 1(c)]

$$\rho_d(\omega) = \frac{1}{2\pi}\frac{1}{\sqrt{\omega_v-\omega}}\Theta(\omega_v-\omega),$$

$$\rho_a(\omega) = \frac{1}{2\pi}\frac{1}{\sqrt{\omega-\omega_c}}\Theta(\omega-\omega_c) \tag{15}$$

with the Heaviside step function Θ. For the EM eigenmode with frequency $\omega \geqslant \omega_c$ (ω_c is the air-band-edge frequency), it belongs to the air band; whereas, for the eigenmode with frequency $\omega \leqslant \omega_v$ (ω_v is the dielectric-band edge frequency), it belongs to the dielectric band. The memory kernels can be determined as

$$K_1(t) = \beta^{3/2} e^{i\pi/4} e^{-i\delta_v t}/\sqrt{t}, \quad K_2(t) = \beta^{3/2} e^{-i\pi/4} e^{-i\delta_c t}/\sqrt{t}. \tag{16}$$

The Laplace transforms of these memory kernels are

$$\tilde{K}_1(s) = \beta^{3/2} e^{i\pi/4}/(2\sqrt{s+i\delta_v}), \quad \tilde{K}_2(s) = \beta^{3/2} e^{-i\pi/4}/(2\sqrt{s+i\delta_c}), \tag{17}$$

which have two singularities exhibiting two dark lines of the SE spectrum [18].

Our aim is to derive the long time spontaneous emission spectrum of the transition $|2\rangle \leftrightarrow \langle 0|$ within the Markovian reservoir, namely, $S(\delta_\lambda) \propto |\alpha_{0\lambda}(t\to\infty)|^2$ with the detuning frequency $\delta_\lambda = \omega_\lambda - \omega_{20}$. The long-time probability amplitude $\alpha_{0\lambda}(t\to\infty)$ could be also obtained from the final-value theorem $\alpha_{0\lambda}(t\to\infty) = \lim_{s\to 0}[s\tilde{\alpha}_{0\lambda}(s)]$ with $\tilde{\alpha}_{0\lambda}(s)$ being the Laplace transform of $\alpha_{0\lambda}(t)$ in Laplace variable s. Through performing the final-value theorem and Laplace transform, we have

$$S(\delta_\lambda) \propto \gamma|\tilde{\alpha}_2(s=-i\delta_\lambda)|^2, \tag{18}$$

with $\tilde{\alpha}_2(s)$ being the Laplace transform of the probability amplitude $\alpha_2(t)$ and given by

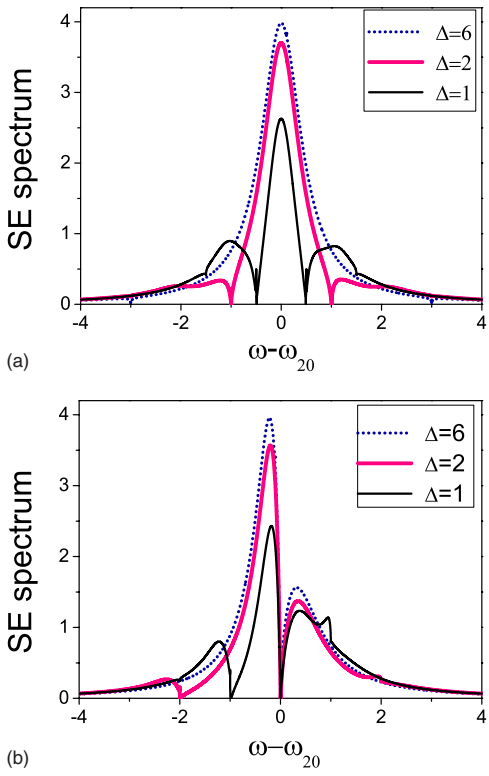

FIG. 3. (Color online) The SE spectra for several gap widths (Δ). The parameters (in units of coupling constant β) are decay rate $\gamma=1$, $\theta(\vec{r}_0)=\pi/4$, PBG width $\Delta=6$ (dotted line), $\Delta=2$ (faint solid line), $\Delta=1$ (dark solid line), and (a) detuning frequency of band edge $\delta_c=-\delta_v=\Delta/2$ for the symmetric cases; (b) $\delta_c=0$, $\delta_v=-\Delta$ for the asymmetric cases ($\delta_c=\omega_c-\omega_{21}$, $\delta_v=\omega_v-\omega_{21}$).

$$\tilde{\alpha}_2(s) = \{1-\sin^2\theta(\vec{r}_0)\cos^2\theta(\vec{r}_0)[\tilde{\alpha}_2(s+iD_\omega)\tilde{K}_1(s+iD_\omega) + \tilde{\alpha}_2(s-iD_\omega)\tilde{K}_2(s-iD_\omega)]\} \times [s+\gamma/2+\cos^4\theta(\vec{r}_0)\tilde{K}_2(s)+\sin^4\theta(\vec{r}_0)\tilde{K}_1(s)]^{-1}, \tag{19}$$

where $D_\omega = \omega_a - \omega_d$ is the frequency difference of the air-band and dielectric-band modes at a fixed wave vector and $\tilde{K}_1(s)$ and $\tilde{K}_2(s)$ are the Laplace transforms of the memory kernels expressed in Eq. (17). We can approximate the frequency difference D_ω by the band gap $\Delta = \omega_c - \omega_v \cong D_\omega$ because most of the PBG density of states (DOS) is contributed from the states near band edges [see Fig. 1(c)]. Here we have applied the Weisskopf-Wigner result [25] to the free-space modes λ and used the iterative method once in this nonlocal difference equation $\tilde{\alpha}_2(s)$ to get the SE spectrum:

$$\tilde{\alpha}_2(s) \cong \tilde{\alpha}_2^{(0)}(s)\{1-\sin^2\theta(\vec{r}_0)\cos^2\theta(\vec{r}_0)[\tilde{\alpha}_2^{(0)}(s+iD_\omega) \times \tilde{K}_1(s+iD_\omega) + \tilde{\alpha}_2^{(0)}(s-iD_\omega)\tilde{K}_1(s-iD_\omega)]\} \tag{20}$$

with $\tilde{\alpha}_2^{(0)}(s) = [s+\gamma/2+\cos^4\theta(\vec{r}_0)\tilde{K}_2(s)+\sin^4\theta(\vec{r}_0)\tilde{K}_1(s)]^{-1}$.

The SE spectra were plotted as a function of detuning frequency $\delta_\lambda = \omega - \omega_{20}$ for several gap widths (Δ) in Fig. 3. The symmetric case in which the atomic transition frequency ω_{21} is chosen at the middle of the gaps is shown in Fig. 3(a).

As expected for the large gap width $\Delta=6$, the excited atom mainly couple to the free-space vacuum and thus the spectrum shows a single Lorentzian peak [18], which is referred to as the free-space light. However, as decreasing the gap width, other than the main peak, we observed two symmetric side lobes separated by zeros, which result from strong coupling of the excited atom through the $|2\rangle \rightarrow |1\rangle$ transition with the PBG reservoir at these two band edges, where we have the largest DOS. The zeros are also termed the dark lines [26]. These two side lobes originate from the atomic free-space transition coupling to the PBG vacuum, which are referred to as the PBG light. This coherent coupling effect grows stronger for the smaller gap widths. For the asymmetric case, in which the atomic transition frequency ω_{21} is located at the air-band edge, the spectrum of the larger PBG is close to that of the single-band case [2,3]; whereas, as decreasing the gap width, the free-space light will be significantly quenched by the atom's emitting the PBG light or loss population through the $|2\rangle \rightarrow |1\rangle$ transition. These results dramatically differ from those of the previous model [18–20], which considered the non-Markovian reservoir as two incoherent PBG reservoirs and showed no intensity quench. Our model reveals, for the smaller gap width, an apparent quantum interference effect (quench in the main peak and enhance dark lines at the band edges) as a result of considering the fields of the non-Markovian reservoir as coherent mode fields. The interference of the free-space light with PBG light from the air band is the same as that from the dielectric band for the symmetric case, whereas it is enhanced in the air band for the asymmetric case (ω_{21} at the air-band edge). Besides, this quantum interference effect also happens when the field modes from the air band interfere strongly with the modes from the dielectric band via the atom. Its result is shown by two shallow kinks of two side lobes for the symmetric case and by an abrupt kink of the right-hand side lobe for the asymmetric case in small gap width $\Delta=1$.

Next, we shall consider how the SE spectrum is affected by the relative position of the atom in a Wigner-Seitz cell which is described by the position-dependent parameter $\theta(\vec{r}_0)$. Both the symmetric case and the asymmetric case were considered for narrow gap ($\Delta=1$) and shown in Figs. 4(a) and 4(b). As increasing the $\theta(\vec{r}_0)$ value, we observed that for both the symmetric and asymmetric cases, the free-space light makes a blueshift with increasing $\theta(\vec{r}_0)$ but does not have much change in intensities. The increase of $\theta(\vec{r}_0)$ causes the growth of the dielectric-band field strength $[\vec{E}^*_{d,\vec{k}} = E_{\vec{k}} \sin\theta(\vec{r}_0)\hat{\epsilon}]$ and thus the stronger coherent coupling with the dielectric-band field to push the free-space light toward the air band. Therefore the interference between the free-space light and the air-band PBG light is then enhanced. It results in the blueshift and increasing radiated power of the air-band PBG light. For the asymmetric case (ω_{21} at the air-band edge), the resonant effect enhances the more radiated power of the air-band PBG light such that the radiated power of the air-band PBG light eventually becomes stronger than that of the free-space light at $\theta(\vec{r}_0)=\pi/3$.

When we consider the system of an ensemble of noninteracting atoms embedded in photonic crystals at symmetry-inequivalent positions with low density per unit cell, the averaged SE spectra shown in Fig. 5 reveal large values of peak-frequency shift. The system with atoms embedded in the dielectric region has blueshift spectra, while those of atoms in air are redshifted. The variation of atomic embedded region results in the spectra shift up to 46.9 [Fig. 5(a)] and 77.8 [Fig. 5(b)] percentage of the half width at the half maximum. This evident phenomenon can be observed in the experimental system of an ensemble of CdSe-ZnSe quantum dots embedded in an inverse opal consisting of air spheres in TiO_2 [27] or ensemble of dye molecules in silica opals [28].

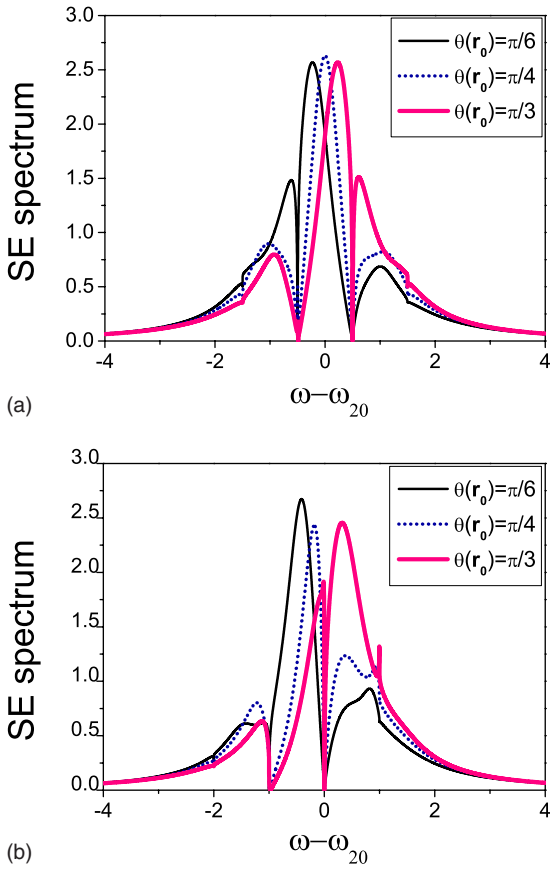

FIG. 4. (Color online) The SE spectra for several atomic position parameters $\theta(\vec{r}_0)$. The parameters (in units of β) are $\gamma=1$, $\Delta=1$, $\theta(\vec{r}_0)=\pi/6$ (dark solid line), $\theta(\vec{r}_0)=\pi/4$ (dotted line), $\theta(\vec{r}_0)=\pi/3$ (faint solid line), and (a) $\delta_c=-\delta_v=0.5$ for the symmetric cases; (b) $\delta_c=0$, $\delta_v=-1$ for the asymmetric cases ($\delta_c=\omega_c-\omega_{21}$, $\delta_v=\omega_v-\omega_{21}$).

The phenomenon of atomic-position dependent spectrum had also been observed experimently by Akahan *et al.* [29]. In order to fabricate a high-Q nanocavity in a silicon-based two-dimensional photonic-crystal slab, they tuned the position of air rods to get a gentler electric field profile at the cavity edges. The peak frequency of the resonant spectrum shifts with the position of the air rods which is shown in Fig. 4. The distribution of the electric field in the cavity is changed because of the movement of the air rods. The air-rods position-dependent spectrum has the same mechanism as that of our result in which atomic position changes field distribution.

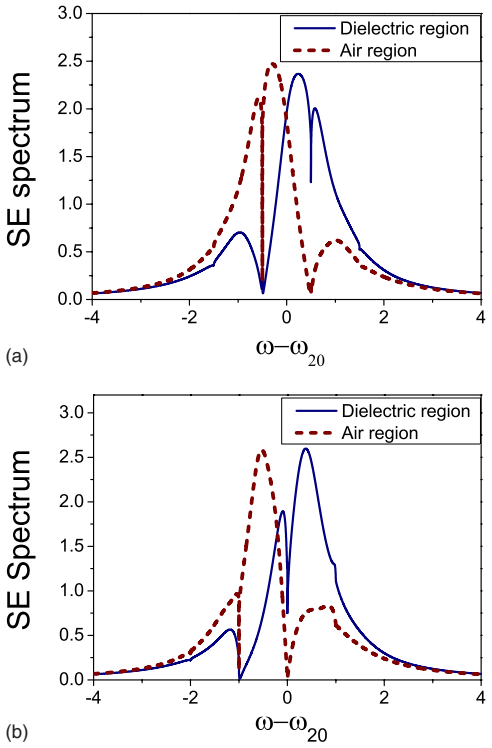

FIG. 5. (Color online) The averaged SE spectra of the system with atoms symmetric-inequivalently embedded in air region and dielectric region. The parameters (in units of β) are $\gamma=1$, $\Delta=1$, $\pi/4 \leqslant \theta(\vec{r}_0) \leqslant 3\pi/4$ for the dielectric region (solid line) and $-\pi/4 \leqslant \theta(\vec{r}_0) \leqslant \pi/4$ for the air region (dashed line), and (a) $\delta_c=-\delta_v=0.5$ for the symmetric cases; (b) $\delta_c=0$, $\delta_v=-1$ for the asymmetric cases ($\delta_c=\omega_c-\omega_{21}$, $\delta_v=\omega_v-\omega_{21}$).

IV. THE ABSORPTION AND DISPERSION FOR A PROBE LASER FIELD

In this section we shall discuss the absorption and dispersion properties of the system by applying a weak probe laser [30] with field angular frequency $\omega \cong \omega_{20}$ to the atomic initial ground state $|0\rangle$. When the perturbed behavior of the system to the probe laser pulse is considered, we add a free-space decay rate γ to the excited state $|2\rangle$ and express the effective Hamiltonian as

$$H = \left[\hbar\Omega e^{i\delta t}|0\rangle\langle 2| + \hbar\sum_a g_a(\vec{r}_0)e^{-i(\omega_a-\omega_{21})t}|2\rangle\langle 1|\hat{a}_a + \hbar\sum_d g_d(\vec{r}_0)e^{-i(\omega_d-\omega_{21})t}|2\rangle\langle 1|\hat{a}_d + \text{H.c.}\right] - i\hbar\frac{\gamma}{2}|2\rangle\langle 2|, \tag{21}$$

where $\Omega=-\vec{d}_{20}\cdot\vec{E}/\hbar$ is Rabi frequency with $\vec{E}$ being the electric field of the probe laser field and $\delta=\omega-\omega_{20}$ is the laser the detuning frequency.

In terms of the "bare" state vector, the wave function is expressed as

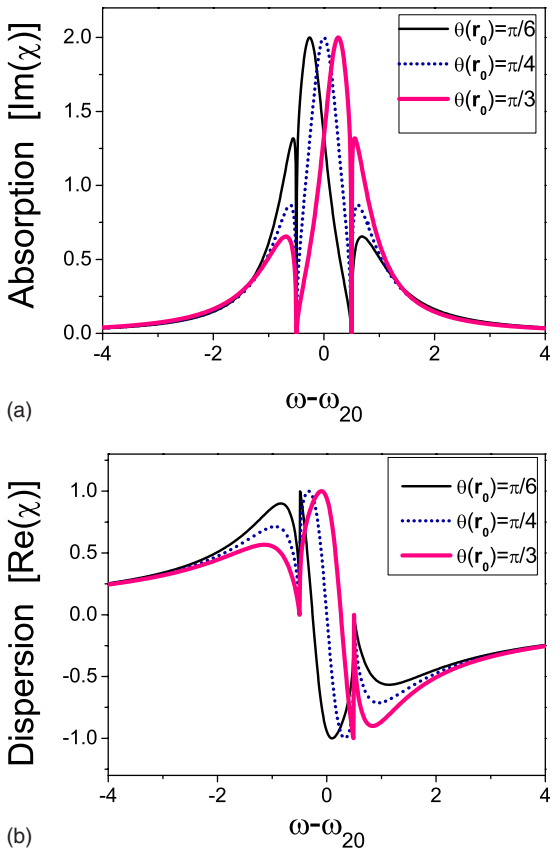

FIG. 6. (Color online) (a) Absorption and (b) dispersion of the system. The parameters are $\gamma=1$, $\delta_c=-\delta_v=0.5$ (symmetry case), $\Delta=1$ (narrow gap), and $\theta(\vec{r}_0)=\pi/6$ (dark solid line); $\theta(\vec{r}_0)=\pi/4$ (dotted line); $\theta(\vec{r}_0)=\pi/3$ (faint solid line).

$$|\Psi(t)\rangle = b_0(t)|0,\{0_a,0_d\}\rangle + b_2(t)e^{-i\delta t}|2,\{0_a,0_d\}\rangle + \sum_a b_{1a}(\vec{r}_0,t)|1,\{1_a,0_d\}\rangle + \sum_d b_{1d}(\vec{r}_0,t)|1,\{0_a,1_d\}\rangle \tag{22}$$

with initial conditions $b_0(t=0)=1$ and $b_2(t=0)=b_{1a}(t=0)=b_{1d}(t=0)=0$. With the same consideration of the coherent reservoir of the system, we applied

$$g_a(\vec{r}_0) = g_{\vec{k}}\cos\theta(\vec{r}_0), \quad g_d(\vec{r}_0) = g_{\vec{k}}\sin\theta(\vec{r}_0) \tag{23}$$

and

$$b_{1a}(\vec{r}_0,t) = b_{1\vec{k}}(t)\cos\theta(\vec{r}_0), \quad b_{1d}(\vec{r}_0,t) = b_{1\vec{k}}(t)\sin\theta(\vec{r}_0) \tag{24}$$

to the position-dependent coupling strength and probability amplitudes. Substituting these equations into the time-dependent Schrödinger equation, we obtained the time evolution of the probability amplitudes

$$i\frac{d}{dt}b_0(t) = \Omega b_2(t), \tag{25}$$

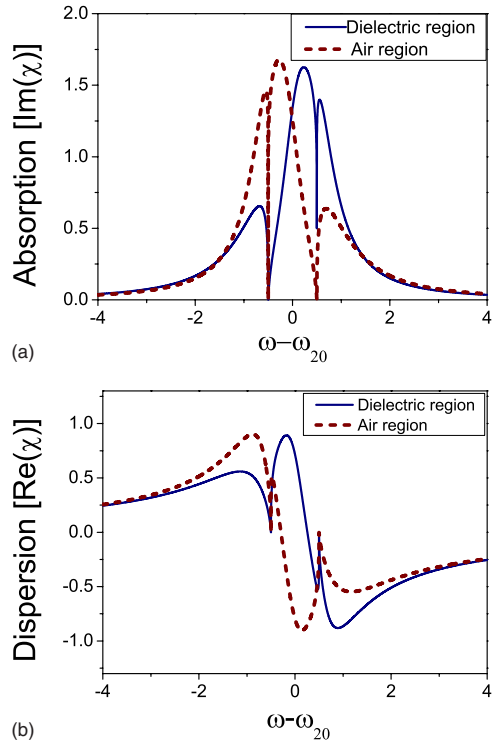

FIG. 7. (Color online) (a) Averaged absorption and (b) dispersion of the system with atoms symmetric-inequivalently embedded in the air region and the dielectric region. The parameters are $\gamma=1$, $\delta_c=-\delta_v=0.5$ (symmetry case), $\Delta=1$ (narrow gap), and $\pi/4 \leqslant \theta(\vec{r}_0) \leqslant 3\pi/4$ for the dielectric region (solid line) and $-\pi/4 \leqslant \theta(\vec{r}_0) \leqslant \pi/4$ for the air region (dashed line).

$$i\frac{d}{dt}b_2(t) = \Omega b_0(t) - \left(\delta + i\frac{\gamma}{2}\right)b_2(t) + e^{i\delta t}\sum_{\vec{k}} g_{\vec{k}} b_{1\vec{k}}(t) e^{-i(\omega_a-\omega_{21})t}\cos^2\theta(\vec{r}_0) + e^{i\delta t}\sum_{\vec{k}} g_{\vec{k}} b_{1\vec{k}}(t) e^{-i(\omega_d-\omega_{21})t}\sin^2\theta(\vec{r}_0), \quad (26)$$

$$i\frac{d}{dt}b_{1\vec{k}}(t) = e^{-i\delta t} g_{\vec{k}} b_2(t) e^{i(\omega_a-\omega_{21})t}\cos^2\theta(\vec{r}_0) + e^{-i\delta t} g_{\vec{k}} b_2(t) e^{i(\omega_d-\omega_{21})t}\sin^2\theta(\vec{r}_0). \quad (27)$$

After substituting a time integral of $b_{1\vec{k}}(t)$ [Eq. (27)] into the time evolution equation of $b_2(t)$ [Eq. (26)] and defining the kernels

$$K_1'(t) = \sum_{\vec{k}} g_{\vec{k}}^2 e^{-i(\omega_d-\omega_{21}-\delta)t} \approx K_1(t)e^{i\delta t},$$

$$K_2'(t) = \sum_{\vec{k}} g_{\vec{k}}^2 e^{-i(\omega_a-\omega_{21}-\delta)t} \approx K_2(t)e^{i\delta t}, \quad (28)$$

we have

$$\frac{d}{dt}b_2(t) = -i\Omega b_0(t) + \left(i\delta - \frac{\gamma}{2}\right)b_2(t) - \int_0^t d\tau b_2(\tau) \times K_1'(t-\tau)\sin^4\theta - \int_0^t d\tau b_2(\tau)K_2'(t-\tau)\cos^4\theta - \int_0^t d\tau b_2(\tau)K_1'(t-\tau)e^{-iD_\omega t}\sin^2\theta\cos^2\theta - \int_0^t d\tau b_2(\tau)K_2'(t-\tau)e^{iD_\omega t}\sin^2\theta\cos^2\theta. \quad (29)$$

Our aim of the absorption and dispersion properties can be obtained from the steady-state linear susceptibility χ of the system. Under the assumption of a weak laser-atom interaction and $|0\rangle \leftrightarrow |2\rangle$ transition occurring in the Markovian reservoir, this linear susceptibility can be expressed as [18]

$$\chi(\delta) = -\frac{4\pi\aleph|\vec{d}_{20}|^2}{\Omega} b_0(t\to\infty)b_2^*(t\to\infty). \quad (30)$$

We assume that the Rabi frequency $\Omega \ll \gamma$ (decay rate), $b_0(t) \approx 1$ for all times, and the atomic-density related constant $4\pi\aleph|\vec{d}_{20}|^2 \equiv 1$ with one embedded atom in the system. Here the long-time behavior of the probability amplitude $b_2(t\to\infty)$ could be resolved from the final-value theorem and the Laplace transform, so the linear susceptibility is

$$\chi(\delta) = -\frac{1}{\delta - i\gamma/2 - i\cos^4\theta(\vec{r}_0)\tilde{K}_2^*(-i\delta) - i\sin^4\theta(\vec{r}_0)\tilde{K}_1^*(-i\delta)} \quad (31)$$

with $\tilde{K}_1^*$ and $\tilde{K}_2^*$ being the complex conjugates of the Laplace transforms of the non-Markovian kernels, which are determined by the PBG model in Eq. (17). The absorption ($-\mathrm{Im}[\chi(\delta)]$) and dispersion ($\mathrm{Re}[\chi(\delta)]$) spectra of the probe field are thus affected by the DOS of the PBG reservoir. Besides, these spectra are also affected by the atomic position inside the PC because of the position-dependent angle $\theta(\vec{r}_0)$.

The absorption and dispersion spectra for the two-coherent-band system were plotted based on Eq. (31) in Fig. 6. The absorption spectra exhibits similar behavior to the spontaneous-emission ones having a central peak with two side lobes and blueshift in the central peak at increasing $\theta(\vec{r}_0)$. The two-band absorption profiles of the atomic-position dependence is shown in Fig. 6(a) for the atomic resonance ω_{21} at the middle of the gap (symmetric case). The transparent windows are independent of the relative position of the atom [$\theta(\vec{r}_0)$] because they are determined by the DOS of the PBG reservoir [18]. As the field strength from the dielectric band of the PBG reservoir grows stronger [$\theta(\vec{r}_0)$ is increased], the central peak of absorption is lying close to the air-band edge (right-hand side). And the absorption on the air-band side lobe is enhanced while the dielectric-band side lobe is suppressed due to coherence coupling and quantum interference effect. As $\theta(\vec{r}_0)$ increases, stronger coupling with the dielectric-band field pushes the free-space absorption line

(central peak) toward the air-band edge. Stronger quantum interference between this central-peak light and the PBG light of the air band enhances the air-band side lobe intensity. This quantum interference effect is due to the coherence of the PBG reservoir, which has a more enhanced effect for the smaller PBG. The coherent property can also affect the transmission of the probe light shown in Fig. 6(b). The frequency of the slow velocity photon shifts toward the blue side for increased $\theta(\vec{r}_0)$. That is, the slow photons with higher frequency represent the stronger coupling with the dielectric-band field. When the experimentally feasible system of an ensemble of noninteracting atoms embedded in the photonic crystal at different region is considered, the averaged absorption spectra shown in Fig. 7(a) also exhibit large values of peak-frequency shift with 49.2% of the half width at half maximum. The frequency shift of the slow photon in the averaged dispersion spectra shown in Fig. 7(b) reaches 57.1% of the peak-to-peak width. This noticeable result could be verified in the experimental system with quantum dots of several nm (4.5 nm) in the air and dielectric region (130–380 nm), respectively, of photonic crystals as in Ref. [27].

V. CONCLUSION

We have studied the effect of atomic position on the spectra of spontaneous emission, absorption, and dispersion of a three-level atom with Λ configuration in a PBG reservoir using the two-band isotropic effective-mass model. With the consideration of the definite phase difference between the air-band and dielectric-band fields, we found that the two-band reservoir is coherent and can interfere with each other. The coupling strength of the atom with this coherent reservoir depends on the embedded position of the atom. This is quite different from the previous two-band studies, which took the PBG reservoir as two independent and incoherent reservoirs and assumed equal strength of coupling between the atom and each individual reservoir of the PBG. Our SE spectra show the coherence phenomenon of the PBG reservoir through the intensity changes of the free-space light and PBG light. Besides, for the small PBG, the spectra of the PBG light reveal quantum interference effect of the PBG reservoir by means of kinks of side lobes. The atomic position-dependent coupling strength is shown by the blue-shift of the free-space light in SE spectra, in which the phenomenon of atomic-position dependent spectra has been observed in experiment [29]. The profiles of the absorption and dispersion show the coherent and quantum interference properties, too. With the variation of atomic position $[\theta(\vec{r}_0)]$, we could observe the coherent property of the reservoir by the shift of the free-space absorption line. The intensity changes of the absorption side lobe illustrate the quantum interference effect of the system with the small PBG. The coherent property could also be observed in the dispersion spectra, whose frequencies of the slow photons vary with atomic position parameter $\theta(\vec{r}_0)$. It results in the change of the refraction index with the atomic position. When we consider the practical system in experiment, the averaged spectra of the system with an ensemble of noninteracting atoms embedded in photonic crystals at symmetry-inequivalent positions show large values of peak-frequency shift up to 77.8% of the half width at half maximum. This consequence is visible in the system of an ensemble of CdSe-ZnSe quantum dots embedded in an inverse opal made of air spheres in TiO_2 [27] or dye molecules in silica opals [28].

ACKNOWLEDGMENTS

We greatly acknowledge partial support from the National Science Council of the Republic of China under Contracts No. NSC 96-2914-I-009-017, No. NSC 95-2119-M-009-029, No. NSC 96-2112-M-034-002-MY3, and No. NSC 96-2628-M-009-001.

[1] R. F. Nabiev, P. Yeh, and J. J. Sanchez-Mondragon, Phys. Rev. A **47**, 3380 (1993).
[2] S. John and T. Quang, Phys. Rev. A **50**, 1764 (1994).
[3] A. G. Kofman, G. Kurizki, and B. Sherman, J. Mod. Opt. **41**, 353 (1994).
[4] T. Quang, M. Woldeyohannes, S. John, and G. S. Agarwal, Phys. Rev. Lett. **79**, 5238 (1997).
[5] S.-Y. Zhu, H. Chen, and H. Huang, Phys. Rev. Lett. **79**, 205 (1997).
[6] Y. Yang, S.-Y. Zhu, and M. S. Zubairy, Opt. Commun. **166**, 79 (1999).
[7] S. Bay, P. Lambropoulos, and K. Molmer, Opt. Commun. **132**, 237 (1996).
[8] S. Bay, P. Lambropoulos, and K. Molmer, Phys. Rev. A **55**, 1485 (1997).
[9] S. Bay and P. Lambropoulos, Opt. Commun. **146**, 130 (1998).
[10] N. Vats and S. John, Phys. Rev. A **58**, 4168 (1998).
[11] S. E. Harris, Phys. Today **50** (7), 36 (1997).
[12] S. E. Harris and L. V. Hau, Phys. Rev. Lett. **82**, 4611 (1999).
[13] M. O. Scully, S.-Y. Zhu, and A. Gavrielides, Phys. Rev. Lett. **62**, 2813 (1989).
[14] L. V. Hau, Phys. World **14** (9), 35 (2001).
[15] S. E. Harris, Phys. Rev. Lett. **62**, 1033 (1989).
[16] N. Vats, S. John, and K. Busch, Phys. Rev. A **65**, 043808 (2002).
[17] J. D. Joannopoulos, S. G. Johnson, J. N. Winn, and R. D. Meade, *Photonic Crystals: Molding the Flow of Light*, 2nd ed. (Princeton University Press, Princeton, NJ, 2008), URL: http://ab-initio.mit.edu/book
[18] D. G. Angelakis, E. Paspalakis, and P. L. Knight, Phys. Rev. A **64**, 013801 (2001).
[19] M. Woldeyohannes and S. John, J. Opt. B: Quantum Semiclassical Opt. **5**, R43 (2003).
[20] S. R. Entezar and H. Tajalli, J. Phys. B **39**, 2959 (2006).
[21] R. Sprik, B. A. van Tiggelen, and A. Lagendijk, Europhys. Lett. **35**, 265 (1996).

[22] For example, if one defines $\theta(\vec{r}_0)=0$ in the middle of the air region of the unit cell, then the middle of the dielectric region of the unit cell corresponds to $\theta(\vec{r}_0)=\pi/2$. Therefore these two coherent fields can be directly read from Fig. 2 once the position of the single active atom is given.
[23] Y. Yang and S.-Y. Zhu, Phys. Rev. A **61**, 043809 (2000).
[24] Y.-S. Zhou, X.-H. Wang, B.-Y. Gu, and F.-H. Wang, Phys. Rev. Lett. **96**, 103601 (2006).
[25] S. John and T. Quang, Phys. Rev. Lett. **74**, 3419 (1995).
[26] E. Paspalakis, D. G. Angelakis, and P. L. Knight, Opt. Commun. **172**, 229 (1999).
[27] I. S. Nikolaev, P. Lodahl, A. F. van Driel, A. F. Koenderink, and W. L. Vos, Phys. Rev. B **75**, 115302 (2007).
[28] R. A. L. Vallée, K. Baert, B. Kolaric, M. Van der Auweraer, and K. Clays, Phys. Rev. B **76**, 045113 (2007).
[29] Y. Akahane, T. Asano, B.-S. Song, and S. Noda, Nature (London) **425**, 944 (2003).
[30] C.-G. Du, Z.-F. Hu, C. F. Hou, and S.-Q. Li, Chin. Phys. Lett. **19**, 338 (2002).

訪問捷克科學院物理研究所

2008.7.30~8.6

楊宗哲

中華大學工程系

1.訪問經過

參加在荷蘭阿姆斯特丹舉行的第 25 屆國際低溫物理會議之前，先到捷克科學院物理研究所作一星期多的訪問研究。由於我與物理所的研究員 Dr. J. Kolacek 及 Dr. Pavel Lipavsky 的共同研究主題都是有關超導的問題，到達布拉格後的隔天，先與 Dr. Lipavsky 討論我的研究問題。然後再討論 Lipavsky 的研究主題－T 矩陣法(BCS 模型下)的修改，使超導與正常態自然地聯接在一起，解釋高溫超導的鷹能隙。此一工作，他正與林佩貞討論，且將送到 PRB 審定中。所以，我們花了一天多的時間。而我所研究的主題是要以雷射脈波去激發高溫超導的 parent 薄膜的 John Teller 模，是這種相干性的高階聲子膜注入高溫超導薄膜裏，使該高溫超導因獲得更多相干性好的 John Teller 模，加強了電子－聲子的耦合作用，而預期會提升更高超導轉變溫度。他建議看 McGill 大學的 Prof。Carbortee 在 70 年代所計算的電子－聲子耦合常數，尤其是$\alpha^2F(\omega)$。不過，我認爲我所關心的是電子經由 high order harmonic ribration modes 耦合，而非電子藉由 harmonic ribration modes 之聲子耦合，其機制需重新探討。在這方面，Kolacek 沒有作出他的看法。不過，我這種看法最近由交大同事告知崔辜琪亦曾提及電子可能是藉由雙聲子耦合。也就是高溫超導的機制，會與聲子有關聯。

我與 Prof. Kolacek 討論他量測 Vortex Mass 的實驗進展情形，及量測 Vortex Mass 的原理和方法。他是採用電容法，二年多來，尚未有多大進展。另外，他還繼續推導超導的電場效應，他想從物理的最基本原理著手去探討，但亦未有多大進展。

在此訪問中，除了學術上的討論外，他們也帶我去捷克西邊的溫泉療養區及全世界唯二之無鉛水晶工廠(Moser)參觀，他們的工藝，除了保留傳統方式之外，仍與德國的 Messen 陶藝工廠合作，開發更新奇的優秀作品，使所生產的水晶維持高價位及高優值。所以其產品通常是歐洲皇宮貴族所喜好收藏，更是捷克總統贈送給外國元首的首選禮物。

2.訪問心得

在這次的短期訪問中，研究部份對我提高T_c的構想思考上，一方面擴大視野，另一方面對自己的構想更加堅定，並繼續發展下去。也期望 Lipavsky 能認同後，大家共同合作去開發。除了研究之外，看到捷克的人文優點，尤其在列強環伺之下，如何生存下去。他們對優秀傳統工藝－水晶，如何發揚光大及保持下去，這是值得我們學習。

3.感謝詞

感謝國科會支助這次的短期訪問。更要感謝捷克科學院物理研究所 Dr. Pavel Lipavsky 給予舒適的住處，讓我能夠欣賞到布拉格全市的美景，也要感謝 Kolacek 夫婦及 Lipavsky 帶我們去優美的溫泉療養區，欣賞美景及人們的優閒的一面。更難能可貴地看到 Moser 工廠生產無鉛水晶的工藝及成品。

Progress in Electromagnetic Research Symposium 2007 Prague (PIERS) 會議報告

楊宗哲中華大學電機工程系

2007.8.27-30　捷克,布拉格(Prague)

會議地點在布拉格,捷克技術大學(Czech Technical University in Prague)

國科會計畫補助編號：
NSC-96-2112—M-216-001

I.會議經過

由於這次會議舉行地點是歐洲歷次大戰中未受災難的城市-布拉格，所以 我就提早幾天到那兒欣賞拉格城市的美，優雅的景色，以前吉布賽人滿街搶劫或強偷的行跡減少太多了、似乎看不到，不過，物價比以前偏高了。我被安排於第一天(8月27日)早上11:20演講”Beam Splitter using a one-dimensional metal photonic crystal with a parabola-like equi-frequency contour”在那個session裡，聽眾很多且許多都是這方面領域的成名專家，問起問題來蠻有趣，且都是要點。

這個會議是有關電磁波近來的新進展，由於每半年一次，參與人數規模約四、五百人左右，大部份是本國人居多，所演講的主題都是近半年來得到的結果.以我為例，一年要參加PIERs二次，新的結果需要半年內至少要有二篇的成果才行，所以，進行的研究很忙。從會議裡可得到很新的靈感，對於規畫研究方向很有幫助，就以本次會議來說，就有一篇報告針對金屬-半導體結構的奇異特性提出新的看法，讓人們有新鮮感及新思維，讓我研究的體系轉入半導體領域，而不是只有金屬的表面電漿子。

Ⅱ.會議內容

此次會議，由於我報告的主題是”Beam Splitter using a one-dimensional metal photonic crystal with a parabola-like equi-frequency contour”它歸納在metamaterical 內。因此專心聽的題目大部份屬於此類。底下就此次會議中，我所聽的一些演講裡，較有心得的主題，大略陳述如下：

(一). A.Sihovola 主講”Geometrically Caused emergence and metamaterials in electromagnetic.”他特別把metamaterial 的定義提出來陳述。Metamaterial 是一物體從其結構而非直接從組成份取得的電磁性質，此一名詞特別用於，不是在自然界所形成的物質。此處的 metamaterials 可作為光及微波的不同應用。

(二). C.T. Chan (香港科技大學)講”Eigenmode analysis of Plasomonic arrays”他介紹他們最近發展出的高效率 eigen-decomposition 方法以分析在金屬奈米顆粒結構裡的電漿子模，此一方法的好處是能同時得到色散關係及模的品質。它也能把材料性質與幾何性質分離出來。所以它的效率不依賴材料的極化率之複雜性。他們運用此方法分析不同結構的金屬奈米顆粒鏈的導引電漿子模。對一維系統，給出

dynamic dipole polarizability，在典型上跟具有輻射修正下的準靜態 dipole polarizability 所得的結果相比較，顯現 red shift 的現象。

(三). F.Urbani 報告他們新近完成的工作，"Wave interaction with double-negative(DNG) and double-positive (DPS)".他們以理論探討 DNG 與 DPS 形成多層膜結構。DNG 板以 Lorentz 及 Drude 介紹參數描述，而 DPS 以已知介電材料定義，以任意偏振的平面波入射到此多層膜材料。運用轉移矩陣法，計算其反射及透射功率，分析在微波，毫米波及光波波段區的高效率濾波器。

(四). Chien-Jang Wu.報告在對稱平面型 反磁/超導/反磁的波導中非線性表面波的傳播性質。他以數值分析在紅外頻段裏，attenuation constant 及 phase constant 隨超導層厚度的變化，發現 attenuation constant 及 phase constant 隨超導層厚度的增加而減小。另外，總功率在傳播常數中，存在臨界值。當傳播常數大於此一臨界值時，電磁波能在波導中傳播。

(五). G.Ghazi，報告"Modal analysis of extraordinary

transmission through sub-wavelength slits in a silver plate"研究結果。他們針對一維狹縫的規則排列，以模匹配得到 eigen-modes，探討通過次波長狹縫的不尋常透射。以這種模分析的手法，決定不尋常透射的不同機制之貢獻，發現在某波長下，入射界面處的被激發的表面電漿極化子能吸收入射功率，因而減小透射功率。

(六). Yu.N.Barabanenkov 報告他們就負折射率材料內，電磁的 evanescent wave 放大及散射的一些現象。Pendry 將 Veselago 的分析予以延伸，證明ε=-1 及μ=-1 的平板左手性材料(LHM)能夠將電磁的 evanescent wave 在穿透時放大，這是因為 evanescent wave 帶有物體(輻射或散射體)次波長的信息，而左手性平板能作為超透鏡，及重構 evanescent wave。他們把 Pendry 的分析工作，再往前展到具有 local inhomogeneity 的 LHM 平板。考慮$\varepsilon(x,z)=-1+\delta\varepsilon(x,z)$，此處$\varepsilon\delta(x,z)$是二維的偏離(即不均勻性)，而$\mu$=-1。他們得到 evanescent wave 受到介電材料的不均勻性散射，卻不影響 LHM 其餘部分在透射時 evanescent wave 放大的能力。

Ⅲ.建議

現在科技發展的版圖，又開始轉到歐洲大陸，尤其蘇聯解體及歐盟經濟的飛躍，使得歐洲各國認識到科技合作發展，以抗衡美國獨大局面，此可由一些創新科學數量上看，歐盟的數量一直在成長，正開始縮短與美國的差距，因此，建議國科會需加重到歐洲參與國際會議及交流。正當美國因反恐策施，使國人至美國開會的不方便性，應該鼓勵去歐洲參與科技合作及交流。

IV.攜回資料

PIERS 2007 Prague 會議議程及論文摘要冊子。其會議論文(部分)所儲存的光碟一片。